CONF-9705114--2

Overview of the National Spallation Neutron Source with Emphasis on the Target Station

Tony A. Gabriel, John N. Barnes, Lowell A. Charlton, James DiStefano,
Ken Farrell, John Haines, Jeffrey O. Johnson, Louis K. Mansur,
Steve J. Pawel, Moshe Siman-Tov, Rusi Taleyarkhan, Mark W. Wendel
Oak Ridge National Laboratory*, P. O. Box 2008, Oak Ridge, Tennessee 37831, USA

Thomas J. McManamy, Mark J. Rennich, Al Williams
Engineering, Lockheed Martin Energy Systems, Inc.,
P. O. Box 2009, Oak Ridge, Tennessee 37830, USA

Presented at
Shielding Aspects of Accelerators, Targets and Irradiation Facilities (SATIF3)
Tohoku University
Sendai, Japan

May 12-13, 1997

*Managed by Lockheed Martin Energy Research Corporation for the U.S. Department of Energy under Contract No. DE-AC05-960R22464.

DISCLAIMER

OVERVIEW OF THE NATIONAL SPALLATION NEUTRON SOURCE WITH EMPHASIS ON THE TARGET STATION

Tony A. Gabriel, John N. Barnes, Lowell A. Charlton, James DiStefano, Ken Farrell, John Haines, Jeffrey O. Johnson, Louis K. Mansur, Steve J. Pawel, Moshe Siman-Tov, Rusi Taleyarkhan, Mark W. Wendel

Oak Ridge National Laboratory, P. O. Box 2008, Oak Ridge, Tennessee 37831, USA

Thomas J. Mcmanamy, Mark J. Rennich, Al Williams

Engineering, Lockheed Martin Energy Systems, Inc., P. O. Box 2009, Oak Ridge, Tennessee 37830, USA

Abstract

The technologies that are being utilized to design and build a state-of-the-art neutron spallation source, the National Spallation Neutron Source (NSNS), are discussed. Emphasis is given to the technology issues that present the greatest scientific challenges. The present facility configuration, ongoing analysis and the planned hardware research and development program are also described.

1.0 Introduction

In many areas of physics, such as materials, biology and nuclear engineering, it is extremely valuable to have a very intense source of neutrons so that the structure and function of materials can be studied. One facility proposed for this purpose is the National Spallation Neutron Source (NSNS). This facility will consist of two parts: 1) A high-energy (~1 GeV) and high powered (~1 MW) proton accelerator (60 Hertz, <1.0 μs/pulse), and 2) A target station which converts the protons through nuclear interactions to low-energy ($\lesssim$2 eV) neutrons and delivers them to the neutron scattering instruments.

This paper deals with the second part, i.e., the design and development of the NSNS target station and the scientifically challenging issues. Many scientific and technical disciplines are required to produce a successful target station. These include engineering, remote handling, neutronics, materials, thermal hydraulics, and instrumentation. Some of these areas will be discussed below.

2.0 Target Station Configuration And Maintenance

The target and experimental systems for the NSNS are located in a single building. As shown in Fig. 1, the target is positioned within an iron and concrete shielding monolith approximately 12 m in diameter. The proton beam enters the mercury target horizontally and the produced neutrons after moderation are used by the scattering instruments. These neutrons exit through 18 neutron beam tubes projecting from the sides. The majority of the 62 m x 83 m building is reserved for the scattering instruments located on the neutron beam lines, however, remote handling hot cells projecting from the back of the shielding are provided for handling the activated target, moderator and reflector components. This region also contains utilities used for the target. Another cell for utility systems is located beneath the main floor level.

Fig. 1 Cutaway view of target facility

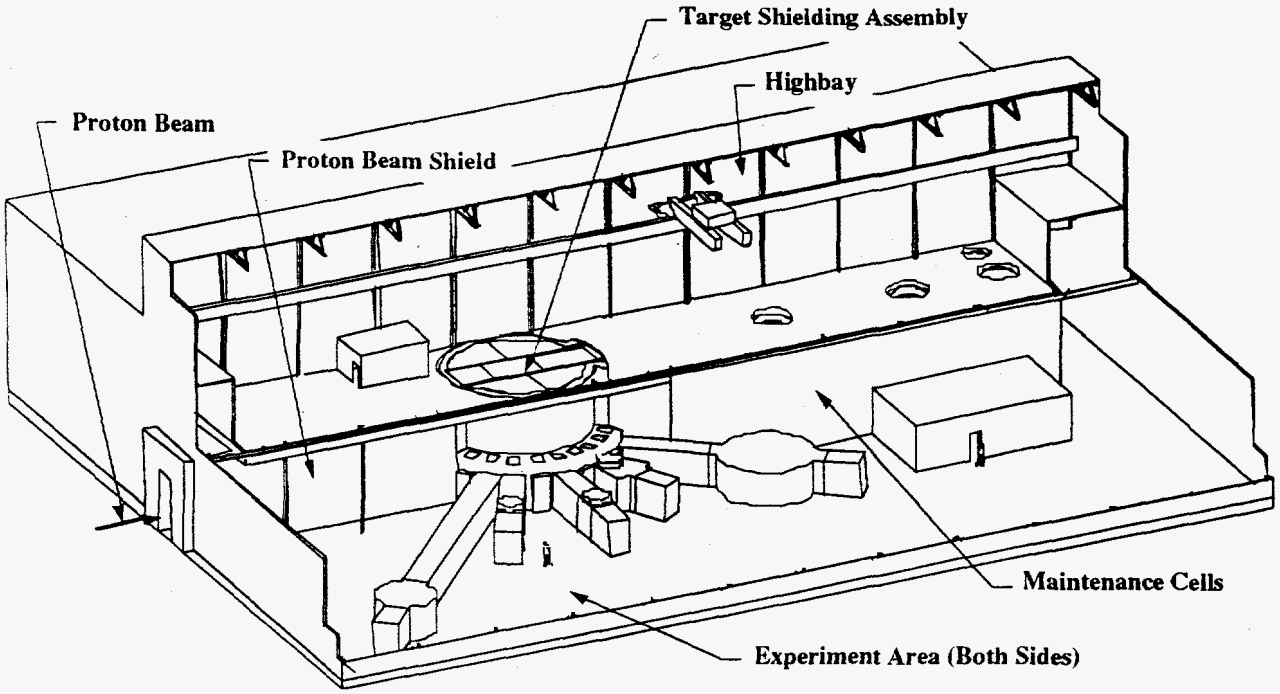

The target facility can be segregated into four areas for discussion:

- target assembly including the moderators and reflectors,
- neutron beam tube systems
- remote handling systems
- target system controls

2.1 Target

2.1.1 Liquid Target Material

The reference design for the NSNS incorporates mercury as its target material. A heavy liquid metal target was selected over a water-cooled solid target because (1) increased power handling capability is possible with a liquid target, (2) the liquid target material lasts the entire lifetime of the facility, and (3) the radiation damage lifetime of a liquid target system, including its solid material container, should be considerably longer. The first advantage is due to the large power loads that can be convected away from the beam-target interaction region with a flowing liquid target. The second advantage results from avoiding the radiation damage that would occur in a solid target material, which eventually leads to embrittlement and fracture of the material. Liquid target vessels will still need to be replaced periodically due to radiation damage to its container structure, but the liquid target material can be reused. The third advantage - longer irradiation lifetime - results from two effects. First, the target structural material used to enclose the liquid target can be selected based on its structural properties and resistance to radiation damage, independent of its neutron production capability, and second, with a liquid target, there is no solid material in the highest neutron flux regions. Therefore the peak displacement damage rate in the window of a liquid target is greatly reduced compared to the peak value in a solid target.

Mercury was also selected as the reference liquid target material because it: (1) is a liquid at room temperature, (2) has good heat transport properties, and (3) has high atomic number and mass density resulting in high neutron yield and source brightness. One significant result from recent neutronic analysis studies has been that the neutron flux from a short-pulse (~1 μs) neutron source is substantially greater for a mercury target than for either water-cooled tungsten or tantalum targets especially at power levels greater than 1 MW (see section 3).

2.1.2 Mercury Target Design Concept

The mercury target design configuration, shown in Fig. 2, has a width of 400 mm, a height of 100 mm, and a length of 650 mm. The mercury is contained within a structure made from 316-type stainless steel. Mercury enters from the back side (side outermost from the proton beam window) of the target, flows along the two side walls to the front surface (proton beam window), and returns through a 224 mm x 80 mm rectangular passage in the middle of the target. Also being considered is the opposite flow, i.e. in through the 224 mm x 80 mm passage and out the two side walls. The target window, i.e., portion of the target structure in the direct path of the proton beam is cooled by mercury which flows through the passage formed between two walls of a duplex structure. In this way, the window cooling and transport of heat deposited in the bulk mercury are achieved with separate flow streams. This approach is judged to be more reliable and efficient (minimal pressure drop and pumping power) than using the bulk mercury to cool the window. Also, the duplex structure used for the window has significant structural advantages that help to sustain other loads. Beside serving as flow guides, the baffle plates used to separate the inlet and outlet flow streams are also important for maintaining the structural stability of the target.

Fig. 2 NSNS Mercury Target

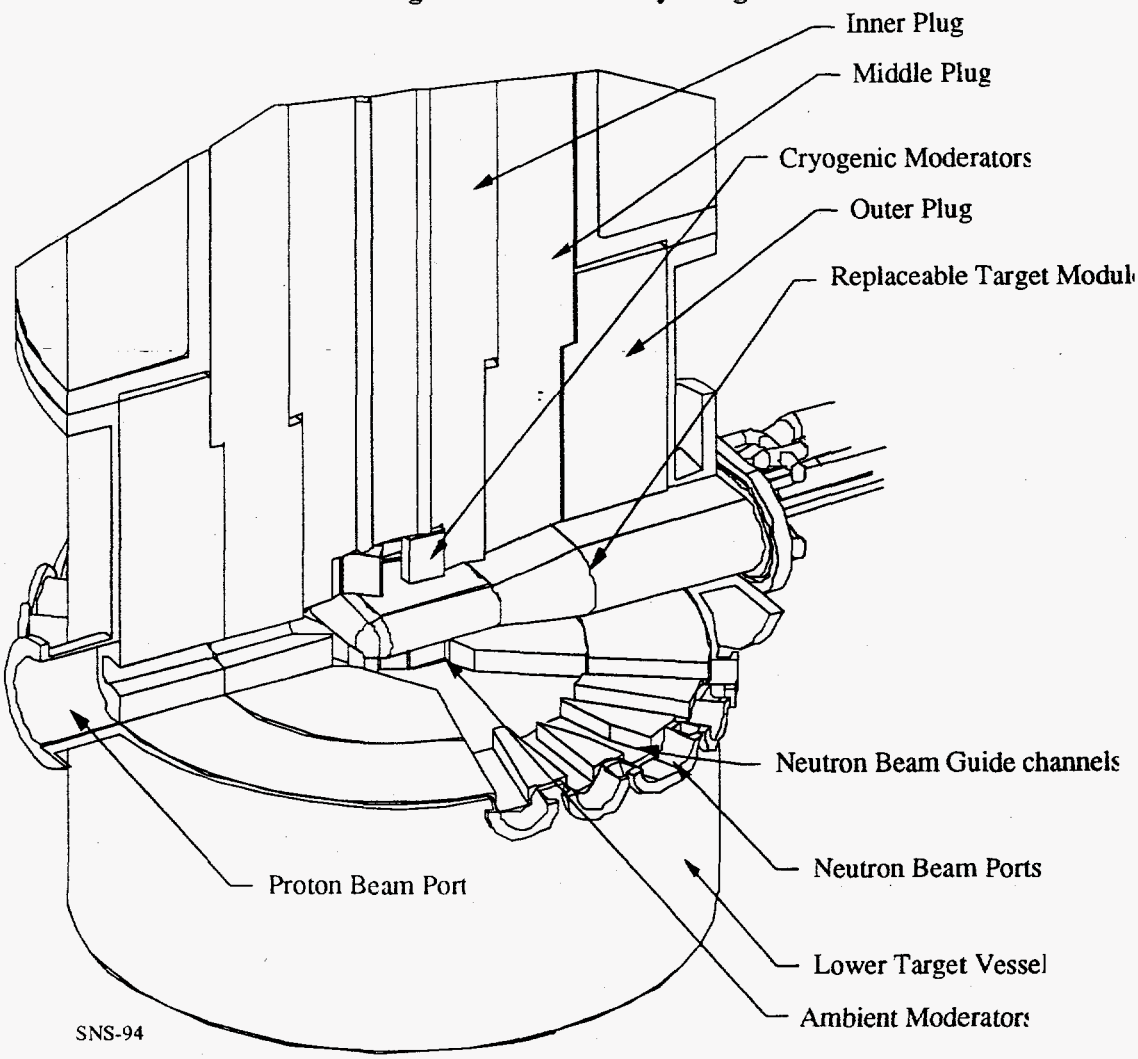

A shroud (safety container) is provided around the mercury target to guide the mercury to a dump tank in the event of a failure of the target container structure. The shroud is a water-cooled duplex structure made from austenitic, 316-type, stainless steel.

2.2 Target Station

2.2.1 Configuration

The overall configuration for the liquid target system is shown in Fig. 3. The mercury target and the water cooled shroud, which are subject to intense interactions with the proton beam, must be replaced on a regular basis. For this reason, all major liquid target system components, except the dump tank, are located on a mobile cart, which is retracted into the target hot cell for maintenance activities. The mercury contained in the target system is drained to the dump tank prior to retracting the target assembly.

The heat deposited in the mercury target is transported away in the flowing mercury loop to a primary heat exchanger that is located on the target cart assembly, outside the target region shielding. The primary heat exchanger is a shell and tube type with mercury flowing in the tube side and the secondary coolant, i.e., demineralized water, flowing in the shell side. The tubes in this heat exchanger are a special, double-walled type which reduces the probability of a mercury leak into the intermediate loop. In addition to this primary heat exchanger, the mercury flow loop also includes piping, valves, fittings, pumps, expansion tanks, and mercury processing equipment. The secondary (water) loop transports the heat to a secondary heat exchanger located in the floor below the target hot cell. The tertiary flow stream utilizes process water.

A water-cooled shroud is provided around the mercury target to guide the mercury to a dump tank in the event of a failure of the target vessel. This shroud is formed from a duplex structure similar to the mercury target vessel and is also made from stainless steel.

The 86-tonne target shield plug, shown in Fig. 3, is designed to shield the equipment located in the target hot cell from the high energy, forward-scattered neutrons produced in the mercury target. The shield plug, which is removed as part of the target assembly during maintenance operations, is constructed from water-cooled, bulk iron encased in a stainless steel liner.

Fig. 3 Target System Configuration

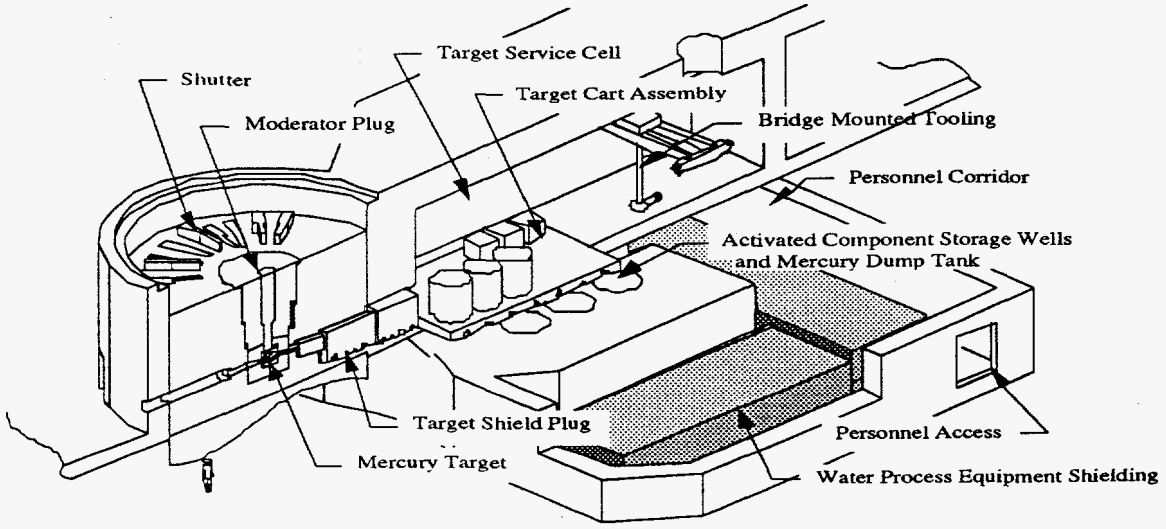

The cart assembly supports all of the mercury flow loop equipment, and provides the means for transporting the target assembly into the target hot cell.

The mercury dump tank is located below all other components in the mercury system thus ensuring that most of the mercury can be drained to the dump tank even in a passive situation (failure of the electric power system). A gas purge system is also utilized under normal circumstances to provide more complete removal of the mercury from the target systems to the dump tank. The capacity of the dump tank is greater than 1 m^3, which is slightly larger than the

mercury inventory in the remainder of the system. The tank is passively cooled by natural convection to remove the nuclear afterheat in the mercury.

2.2.2 Ambient Temperature Moderators

Figure 2 shows the two light-water moderators planned for the NSNS. They are located in wing geometry below the mercury target and water-cooled shroud. The moderator vessel is made from aluminum alloy-6061. The upstream moderator has a thickness of 50 mm, relative to the proton beam, and is decoupled and poisoned to give high temporal resolution of the neutron flux. The second moderator is 100 mm thick and is coupled to produce higher neutron intensity but with less temporal resolution. Both moderators are approximately 120 mm wide and 150 mm high.

The overall heat load in the ambient moderators is estimated to be 4 kW (2 kW per moderator) based on calculations carried out for the NSNS design and on extrapolations from ISIS and ESS data. This heat load results in an overall temperature rise of less than 1 °C for a nominal flow rate of 2 L/s.

2.2.3 Cryogenic Moderators

In addition to the two ambient temperature moderators located beneath the target, two cryogenic moderators, cooled with supercritical hydrogen, are located above the target as shown in Fig. 2. This configuration improves the cooling and warming characteristics of the moderators. Mechanically circulated supercritical hydrogen gas at a pressure of 1.5 MPa was chosen for the moderators because it improves the cooling operation, eliminates boiling and adds flexibility in operation. The hydrogen is maintained at supercritical pressures in all parts of the loop during normal operation.

2.2.4 Reflector Systems

As identified in Fig. 2, the reflector system consists of three plug assemblies, namely the inner reflector, middle plug, and the outer reflector. The inner plug consists of a stainless steel case packed with beryllium rods and cooled with heavy water and holds all four moderators. Neutron decouplers made from boral are mounted on the inner surface of the case. The heavy water flow loop includes appropriate equipment, such as piping, valves, an expansion tank, connectors, pumps, ion exchangers, and instrumentation. The system is designed with connectors to allow disconnection and removal of the reflector assembly vertically into a shielded cask for transport to the target assembly hot cell.

A middle plug holds the majority of the beryllium reflector and is similar in construction to the inner plug. The outer plug consists of nickel shielding with water cooling within a steel case and is contained within a 2 m diameter safety vessel.

2.2.5 Neutron Beam Transport Systems

The neutron beam tube systems provide the paths for moderated neutrons to travel through the bulk shielding to the scattering instruments. The configuration assumed at present consists of 18 beam lines looking at the four moderators as shown in Figs. 1 and 2. Each moderator face which is viewed illuminates three beam lines, one normal to the face and two at plus or minus 13.75 degrees. The upper and lower forward moderators have two faces viewed and the two rear moderators each have one face viewed for a total of 6 viewed faces. This arrangement allows a 70 degree arc for the proton beam entrance region and a similar 70 degree arc for the remote maintenance systems at the rear of the target.

A neutron beam shutter concept similar to the ISIS vertical shutter design is planned. The shutters are in the form of stepped rectangular slabs. In the open position a hole in the shutter aligns with the neutron beam flight path and cross section. The shutter is lowered approximately 500 mm to close. This puts approximately 2 m of heavy shielding (W or Ta) in the neutron flight path. The drive for the shutters will be located at the top. Each shutter will be made from several sections to reduce the height above the top of the bulk shielding required for removal and the size of the shielded flask required for transport. All shutters will be the same, except for the

difference in beam elevation required between beam lines viewing the upper or lower moderators. The weight of one shutter assembly is approximately 25 tonnes.

The neutron beam lines require shielding outside of the bulk target shield. This shield is both for personnel protection and also to reduce the background noise in instruments. It is assumed that standard modules will be developed to allow sections to be added or removed, depending on the requirements and locations of the scattering instruments.

2.2.6 Remote Handling Systems

Optimization of both the operating availability and predictability, while protecting personnel, is the primary goal of the maintenance systems for NSNS. Several techniques proven in successful facilities throughout the world are applied to assist the operators in meeting the operating goals. These include designing equipment from the earliest stages to reduce the need for remote handling. Operating equipment are packaged in modular assemblies designed to be replaced with on-site spares. This enables operations to continue while time-consuming repairs are performed in off-line facilities.

The As Low As Reasonably Achievable (ALARA) principle is used as guidance for all personnel and contamination control operations in NSNS. Thus, activated and contaminated equipment are shielded for transport around the facility and to the permanent storage site. Areas of potential contamination are isolated by seals and valves. Repair and replacement of active components are accomplished in the hot cell adjoining the target shielding stack as identified in Fig. 3.

A target service cell is located behind the target assembly for the purpose of maintaining the highly activated target components. It measures 10 meters wide by 17.8 meters long by 8 meters high. All work is performed via remote handling techniques behind concrete shielding walls. Conventional remote handling tools such as telerobotic manipulators, CCTV and special lighting are used to assist with the replacement of target components. Modular packaging of the components is used to reduce downtime.

A general maintenance cell is located behind the target service cell primarily to maintain the moderator/reflector plug, proton beam window, neutron guide tubes and shutters. Generally all operations will be remote; however, personnel may enter the cell following extensive cleanup. The cell measures 10 meters wide, 10.9 meters long and 9.5 meters high.

The enclosed, unshielded high-bay above the target system and maintenance cells will provide the primary means of handling components in the target system. It measures 12 meters wide, 20 meters high and extends 55 meters. A 50 tonne bridge crane provides access to all of the maintenance cells, storage wells and the transportation bay. The access bay is normally accessible to personnel, consequently all activated components will be shielded and contained during operations and during component transfers between the hot cells. In addition, utility and instrument connections to the vertical access plugs (i.e. shielding, moderators, reflectors and proton beam window) are routed in shielded trenches in the floor of the bay.

3.0 Neutronics

The neutronic behavior of the target system can be obtained by using Monte Carlo techniques to track the progress of various subatomic particles as they proceed through the target. For the work presented here the codes HETC95 [Ref. 1] and MCNP [Ref. 2] were used. The codes were coupled in order to provide the proper source for the low-energy MCNP calculations. Various parameters were calculated to measure the neutronic performance of the target design. The two parameters which were most often tracked in the study reported below were the neutron current (J) passing into the neutron beam channels which lead to the experimental area and the time width (W) of the beam channel neutron pulse.

For this first study, a proton energy of 1.7 GeV, a power of 1 MW, a repetition rate of 60 Hz and a proton pulse width of .5 μs was assumed. The target assembly is shown in Fig. 4. The beryllium reflector surrounds the neutron-producing mercury target, the moderators, which slow the produced neutrons to useful energies (the top cryogenic moderators are filled with liquid hydrogen and the bottom ambient moderators with water), and the neutron beam channels which

Fig. 4 Target assembly enclosed in the Beryllium reflector.

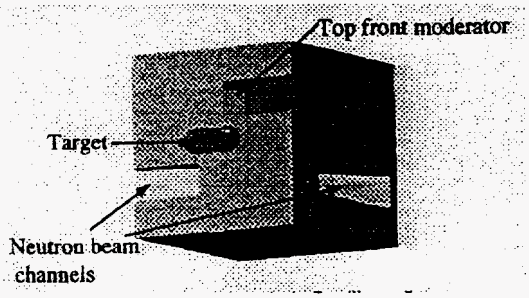

guide the neutrons to the experimental area. In Fig. 4, the beryllium has dimensions 0.9 m x 0.9 m x 1.008 m with the square plane perpendicular to the proton beam direction. The largest dimension of the proton beam channel is 120 mm by 320 mm. In Fig. 5 the target assembly is shown as viewed from the bottom with the reflector material removed. The target, neutron beam channels and the bottom ambient moderators feeding the neutron beam channels can be seen. Two cryogenic moderators are located on the top of the target in analogous positions. The mercury target in Fig. 5 is 640 mm long with a half cylinder of radius 50 mm on the end where the proton beam enters (to the right in the figure). Downstream from the half cylinder is a section with rectangular cross section width of 300 mm and a height varying from 100 mm upstream to 150 mm at the extreme downstream end. Various moderator parameters are shown in Table 1.

Fig. 5 Target, moderators, and the neutron beam channels as viewed from the bottom.

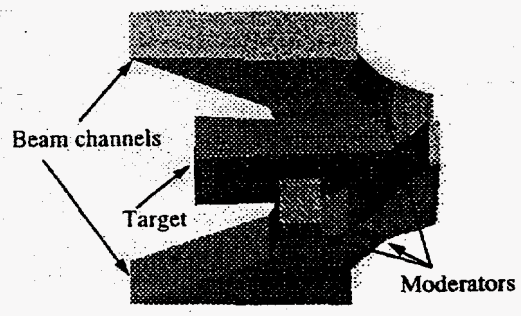

In the sections to follow a comparison between Hg target performance and that of W and Ta is given. Also, results showing the effect on moderator performance of poisoning (inserting a thin layer of gadolinium into the moderator center parallel to the exit face(s)), and decoupling(surrounding the moderator and reflector with cadmium on all sides except those through which the neutrons exit) will also be presented along with a comparison of the calculated neutron spectrum with an analytic form which will facilitate optimization of the target.

3.1 Mercury Target

The preferred target for NSNS is mercury. This choice is motivated by anticipated advantages in many areas. The neutronic superiority of Hg over two other commonly considered targets is shown in Table 2. This increase in neutronic performance will be slight at 1 MW but substantial at 5 MW due to the increase in the H_2O cooling needed for the solid target at 5 MW. The hydrogen in the water thermalizes some of the neutrons within the W or Ta target area. Since both W and Ta have large capture cross sections these thermalized neutrons are captured and therefore lost. Calculations of the neutron flux for a 5 MW target station are shown in order to facilitate a comparison with a different study done for ESS. The results of this study are also shown. As may be seen, Hg gives a larger neutron flux than either Ta or W. This is true for both

cryogenic (liquid H_2) and ambient (H_2O) moderators. Comparison of the neutron spectrum and pulse showed virtually identical characteristics except for the additional neutrons given by the Hg target.

3.2 Moderator Enhancement

It is desirable to maximize the neutron current (J) emerging from the moderator and to minimize the time width (W) of the neutron pulse. The results discussed in this section concern the use of moderator poisoning and moderator decoupling to reduce the time width of the neutron pulse. These methods successfully reduce the width but they also reduce the neutron current. Thus a trade off is required between the neutron current and the width of the pulse. The best trade off is determined by the target output requirements.

Table 1 Moderator Parameters (unless stated otherwise in text)

Moderator	Dimensions (mm)	Decoupler Thickness (mm)	Poison Thickness (mm)
Top Upstream (Faces 1&2)	120 x 150 x 50	1. Cd	0.05 Gd
Top Downstream (Faces 3&4)	120 x 150 x 50	1. Cd	0.05 Gd
Bottom Upstream (Face 5)	120 x 150 x 50	1. Cd	0.05 Gd
Bottom Downstream (Face 6)	120 x 150 x 100	1. Cd	0.05 Gd

The size of the moderator face from which the neutrons enter the beam channel is given by the first two dimensions in the second column.

In order to better understand the width reduction produced by each method, the energy distribution produced will be shown first. In Fig. 6, the number of neutrons per incident proton leaving a moderator face is shown versus the energy in meV. The face used is one of the two on the front top cryogenic moderator (the two faces yield virtually identical results). Both poisoning and decoupling reduce the neutron current and using both reduces it further than using either separately. Poisoning (accomplished by gadolinium with a cut-off energy of .1-.2 eV) changes the neutron spectrum only for energies $\lesssim$ .1-.2 eV. Neutron capture in Gd above this energy is small. It may also be seen that decoupling modifies the neutron spectrum only for energies below the cadmium cut-off energy of ~.4-.6 eV.

These same effects can be seen for the ambient moderators except they are much less pronounced. This is because the peak in the energy distribution is located at a much higher energy relative to the cut-off energies of both cadmium and gadolinium which means that a much smaller proportion of the neutrons that eventually moderate to the peak energy are affected by the poisoning and the decoupling. This produces a smaller effect. The threshold for decoupling occurs at the cut-off energy for cadmium and the threshold for poisoning occurs at the cut-off energy for gadolinium. These thresholds are, however, much farther above the peak in the coupled energy distribution for the cryogenic moderator than for the ambient moderator.

The change in the shape of the neutron pulse for the cryogenic moderator due to poisoning and decoupling can be seen in Fig. 7. The decoupling and poisoning preferentially affect the low energy particles which take longer to reach the moderator face. At small times all pulses are approximately the same. Only at large times do the poisoning and decoupling reduce the current and thus produce a smaller time pulse width as desired. The changes produced when an ambient moderator is considered are again smaller than for the cryogenic case. This is due to the same reasons discussed above. Time pulse distributions have also been calculated for various energy ranges, for example, 10 to 20 meV.

Table 2 Comparison of thermal neutron fluxes at the moderator faces for Hg, W and Ta Targets at 5 MW

Cryogenic				
	NSNS		ESS	
Target	ϕ_{th}	R	ϕ_{th}	R
Hg	2.94×10^{14}	1.35	3.91×10^{14}	1.23
W	2.54×10^{14}	1.17	3.53×10^{14}	1.10
Ta	2.17×10^{14}	1.00	3.19×10^{14}	1.00

Ambient				
	NSNS		ESS	
Target	ϕth	R	ϕth	R
Hg	3.35×10^{14}	1.35	2.29×10^{14}	1.51
W	2.91×10^{14}	1.17	1.67×10^{14}	1.10
Ta	2.48×10^{14}	1.00	1.52×10^{14}	1.00

Units: ϕ_{th} ($n \cdot cm^{-2} \cdot s^{-1}$)

ESS results from D. Filges, R. D. Neef, and H. Schaal "Nucl. Studies of Different Target Systems for ESS," ICANS-XIII.

NSNS "effective" fluxes were converted from 2π steradian current calculations. The differing distances from the target to the moderator were also corrected for.

R is the ratio of the flux from the given target to that from a tantalum target.

Fig. 6 Neutron energy distribution from the face of the front cryogenic moderator, C = coupled, P = poisoned, D = decoupled, P-D = poisoned and decoupled

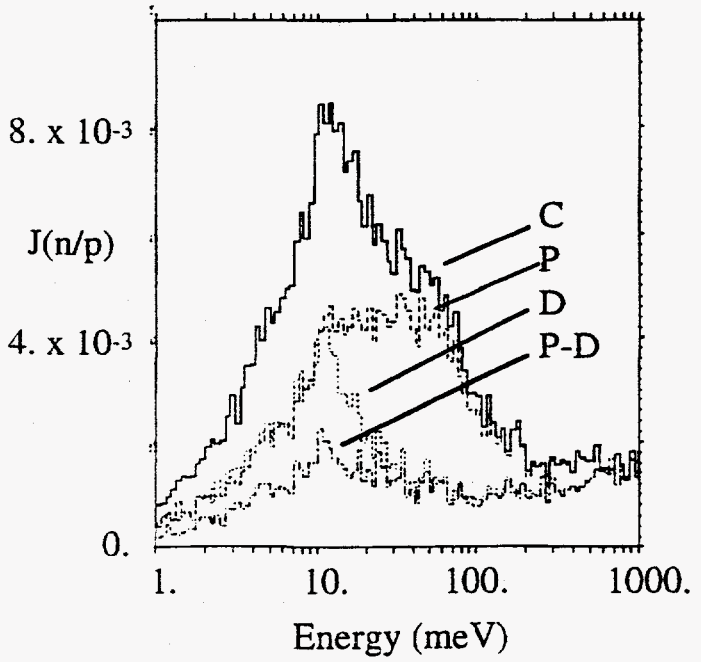

Fig. 7 Thermal neutron pulse from the face of the front cryogenic moderator.

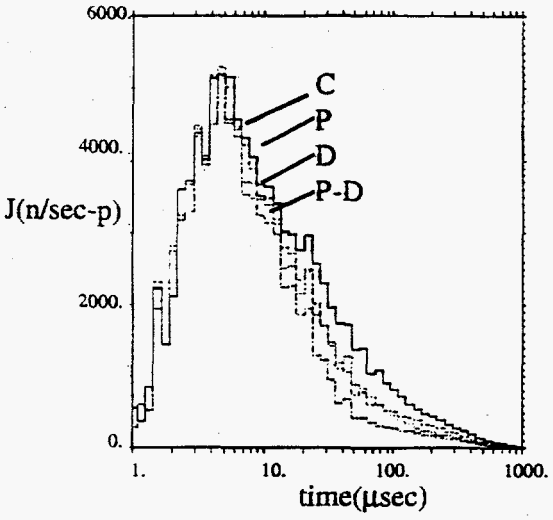

Table 3 Maximum (J_{mx}) and Average (J_{av}) Currents and Pulse Widths (W) for the Front Cryogenic (Faces 1 and 2) and the Front Ambient (Faces 3 and 4) Moderators (Note that 2π current is given instead of 4π flux which can make the values appear a factor of ~4 smaller)

Neutron Currents and Pulse Widths						
	Coupled			Decoupled and Poisoned		
Face	J_{av} $(n \cdot cm^{-2} \cdot s^{-1})$	J_{mx} $(n \cdot cm^{-2} \cdot s^{-1})$	W (μs)	J_{av} $(n \cdot cm^{-2} \cdot s^{-1})$	J_{mx} $(n \cdot cm^{-2} \cdot s^{-1})$	W (μs)
1	6.73×10^{12}	9.53×10^{14}	38	1.90×10^{12}	8.17×10^{14}	15
2	6.66×10^{12}	9.20×10^{14}	38	1.73×10^{12}	7.83×10^{14}	14
3	7.06×10^{12}	1.74×10^{15}	30	3.28×10^{12}	1.60×10^{15}	17
4	7.87×10^{12}	1.91×10^{15}	26	3.97×10^{12}	1.80×10^{15}	17

The total currents from the moderator faces together with the pulse widths are shown in Table 3.

3.3 Analytic Expression for the Neutron Current

An analytic expression is given in Ref. 3 for the neutron current from a moderator face (this expression was originally from Ref. 4). This analytic expression equates the neutron current (J) to a product of two factors. One of these factors depends on the moderator parameters and the other on the source of neutrons to the moderator. This offers the possibility of decoupling the performance of the moderator from that of the source thereby allowing an approximate separate optimization. The expression is

$$J(E) = S\, M(E)$$

with M(E) depending on moderator parameters and S depending on the source. Specifically,

$$M(E) = \left[\left(I_{th} / I_{epi}\right)\left(E / E_T\right)^2 \exp\left(-E / E_T\right) + \Delta(E)E^{\alpha}\right],$$
$$S = I_{epi} = J(E)\big|_{1eV},$$
$$\Delta(E) = \left[1. + (5E_T / E)^{\beta}\right]^{-1} \qquad (1)$$

where

$$\alpha = .2,\ \beta = 7, \qquad E_T = kT_{eff},$$

E is the neutron energy,
I_{th} is the total thermal neutron beam current and
T_{eff} is an effective temperature somewhat greater than the physical temperature of the moderator.

A comparison (Fig. 8) between this expression and the neutronic current given by the Monte Carlo calculations shows excellent agreement for the ambient moderator face and reasonable agreement for the cryogenic moderator face.

The success of the analytic separation into a moderator factor and a source factor is shown in Fig. 9. At the top the spectrum from the ambient moderator is compared to that from the cryogenic moderator. These two moderators are placed symmetrically with respect to the Hg target in the target assembly model as indicated in Fig. 5. The differences in the neutron current should be due only to the moderators themselves. The analytic expression implies that the currents from each moderator should thus be the same at 1 eV, as is true from the figure. At the bottom of the figure the moderators are identical but are placed at different distances above the Hg target. Thus the differences in the neutron current should be due to the source of neutrons to the moderators. The analytic expression would then predict that the neutron spectra from the two targets should differ by a constant (the constant being the neutron current at 1 eV). The plot at the bottom of the figure compares the spectrum from target 1 to the spectrum from target 2 scaled by 1.25. As predicted by the analytic expression they are (within statistics) the same. Thus the analytic treatment should provide a method of approximately optimizing the moderators separately from the rest of the target station.

3.4 Summary and Conclusions for the Neutronics

A Hg target is neutronically better than W or Ta, especially at the higher (>1 MW) power levels where the solid targets need more cooling water.

When a target, moderator and reflector are selected together with the geometry, the order of magnitude of the neutron current and the pulse width are determined. The results in this paper found methods which changed these neutronic properties by, at most, a factor of ~5. Thus, if a change in moderator performance of >10 is required methods other than those discussed here are needed.

It was also found that using a combination of decoupling and poisoning produced different results for an ambient moderator than for a cryogenic moderator. For an ambient moderator the pulse width could be reduced by a factor of ~2 which also resulted in a reduction in the neutron current of ~2. For a cryogenic moderator, the pulse width and current reduction was ~3.

An analytic expression was shown which should allow a better optimization process. It should be emphasized that the target used in this study was a "first try" in a design study for NSNS and does not represent a final configuration. It is anticipated that most of the results found, however, will have a very general applicability and, for the most part, the "lessons" learned will apply in finding the best target configuration. The absolute latest neutronic results can be found in a paper by L. A. Charlton which is published in these proceedings.

Fig. 8 Comparison of spectra from a Monte Carlo calculation using MCNP and the analytic expression. This comparison is for a H_2O moderator (top) and a liquid H_2 moderator (bottom).

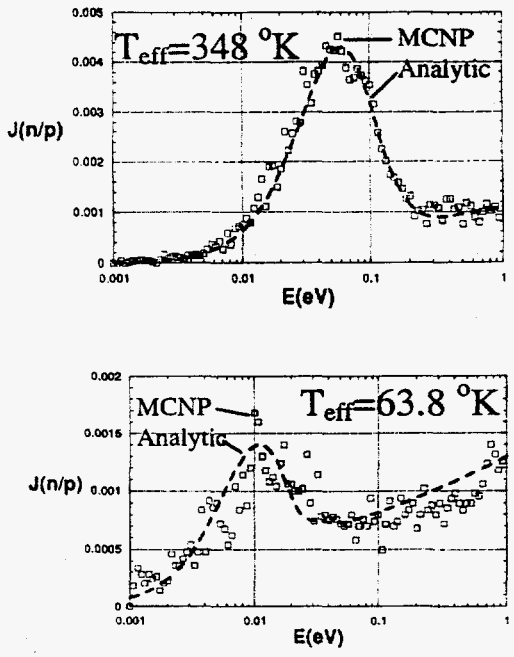

Fig. 9 Spectra showing the success of the analytic model. The spectra at the top are identical at 1 eV as predicated by the model. The spectra at the bottom are identical except for an overall normalization. This is also predicted by the model.

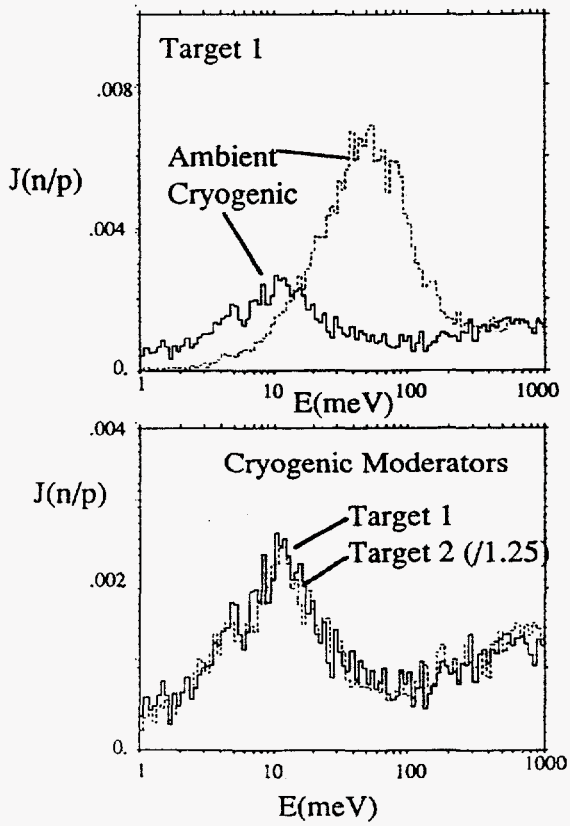

4.0 TARGET RESEARCH

4.1 Mercury Target Performance Evaluations

The mercury target and its enclosing structure must be designed to sustain the time-averaged power loads as well as the nearly instantaneous power deposition during single pulses. These time-averaged and single pulse loads are defined in Table 4. Since about 60% of the proton beam power is deposited in the target, the thermal-hydraulic system for the target is designed to remove a time-averaged power of approximately 0.6 MW corresponding to a proton beam power of 1 MW. Since the pulse frequency is 60 Hz, the amount of energy deposited in the target during a single pulse is about 10 KJ.

Table 4. Power loads on the NSNS mercury target

Parameter	Value
Energy of protons (GeV)	1
Pulse duration (μs)	0.5
Pulse frequency (Hz)	60
Percent of beam power deposited in mercury target (%)	~ 60
Time-Averaged Loads	
Beam current (mA)	1
Total proton Beam Power (MW)	1
Peak current density on target (A/m^2)	0.1
Peak beam power flux on target (MW/m^2)	
Peak volumetric heating rate in mercury (MW/m^3)	640
Peak volumetric heating rate in window (MW/m^3)	336
Loads During a Single Pulse	
Energy per pulse (kJ)	~10
Peak energy density in mercury (MJ/m^3)	10.7
Peak energy density in window (MJ/m^3)	5.6

4.2 Handling of the Time-Averaged Power

The power deposited in the target must be transported away without excessive mercury or stainless steel vessel temperatures or stresses. This is achieved using two separate mercury flow streams; one to transport the heat deposited in the mercury contained in regions interior to the vessel, and one to cool the stainless steel vessel structure. Three-dimensional computational fluid dynamics (CFD) simulations of the target main flow and the cooling jacket were performed using the general purpose CFD code CFDS-FLOW3D [Ref. 5].

In the main mercury target flow stream, mercury enters the target through the two side channels at 80 °C with a flow rate of 146 kg/s. The resulting bulk (volume averaged) temperature rise in the mercury is 30 °C. As shown in Fig. 10, the power deposited in the bulk mercury is effectively transported from the target with reasonable flow rates, pressure drop, and pumping power. The maximum temperature in the bulk mercury is less than 160 °C. Temperatures in the recirculation zone located near the flow baffles are less than 150 °C because the heating rate for the specified parabolic profile is relatively low in this region.

As illustrated in Fig. 11, a mercury flow rate of 14 kg/s in the cooling jacket provides adequate cooling for the stainless steel vessel. The inlet temperature is 80 °C, and the temperature rise through the coolant passages formed by the two walls of the duplex structure is

Fig. 10 Flow and temperature distributions in a preliminary mercury target design concept for a 1 MW proton beam (entire target cross section shown).

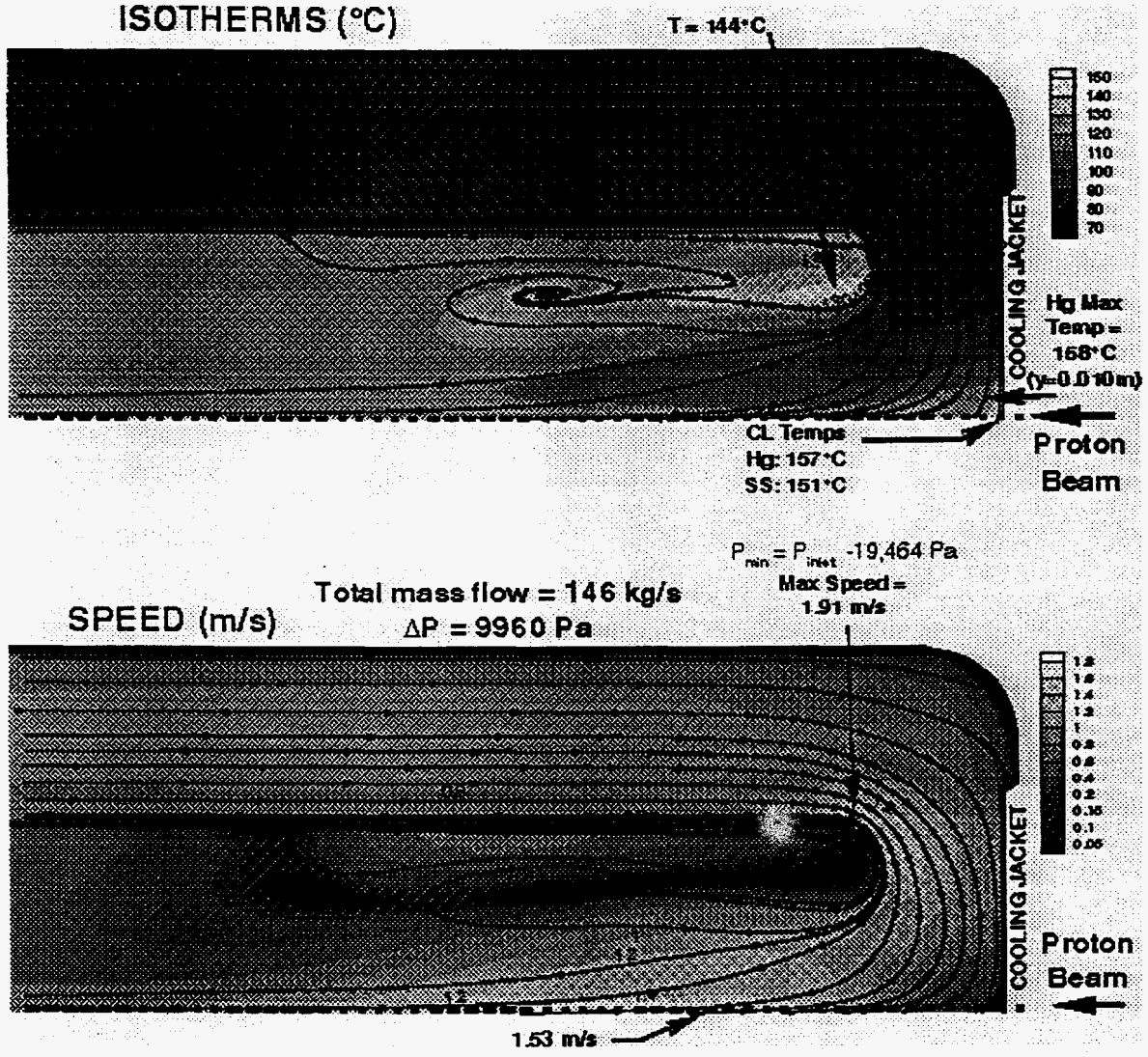

estimated to be less than 30 °C (varies with passage location). The maximum stainless steel temperature on the target vessel wall is less than 170 °C assuming good thermal contact or wetting of the mercury on the stainless steel wall. This temperature is judged to be acceptable from the materials compatibility viewpoint and is well below limits associated with excessive loss of strength or other mechanical properties.

4.3 Evaluation of the Thermal-Shock Loads

The interaction of the energetic proton beam with the mercury target leads to very high heating rates in the target. Although the resulting temperature rise is relatively small (a few °C), the rate of temperature rise is enormous (~10^7°C/s) during the very brief beam pulse (~ 1 μs). The resulting compression of the mercury will lead to the production of large amplitude pressure waves in the mercury that interacts with the walls of the mercury container, and the bulk flow field. Concerns exist in two main areas, viz., (1) impact of the effects of the combination of thermal shock on the wall due to its direct heating from the proton beam and the loads

Fig. 11 Temperature and velocity profiles in the central channel of the target vessel cooling jacket for a 1 MW proton beam.

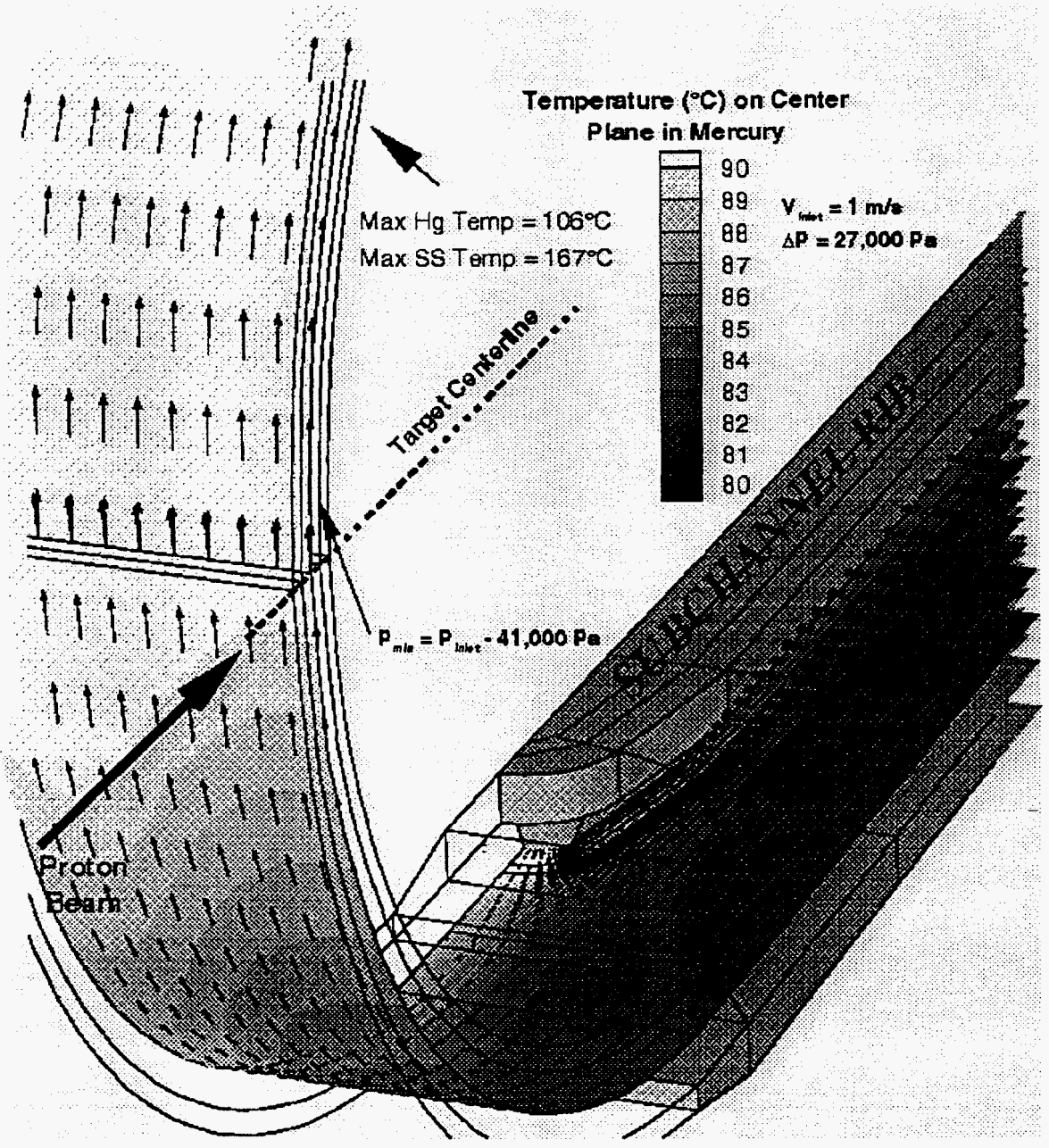

transferred from the mercury compression waves, and, (2) impact of the compression-cum-rarefaction wave-induced effects such as fluid surging and potential cavitation. This has led to the conclusion that tests and analyses are required before using a liquid target (mercury) in the intense thermal load environment expected for a pulsed spallation neutron source.

The capability to understand and predict the propagation of the pressure pulses in the target (either liquid or solid) is considered to be critical for designing and constructing such a device. The CTH code [Ref. 6] system developed at Sandia National Laboratory is being used to model this situation. CTH is a three-dimensional, shock-physics code, sometimes loosely referred to as a hydrocode. ORNL has developed significant expertise and related technology in use of this modeling framework to simulate explosive processes (such as molten metal-water vapor explosions) in enclosed fluid-structure systems. This technology is being used for characterizing the current thermal-shock process in a coupled manner, simultaneously accounting for localized compression pulse generation due to rapid heat deposition, transport of the compression wave

through the mercury, interaction of this wave with the surrounding structure, feedback to the mercury from these structures, and multi-dimensional reflection patterns including rarefaction-induced material fracture (or possible cavitation phenomena in fluids).

Whereas, a full-scale three-dimensional model for the NSNS target is under development, modeling efforts so far have examined the effects of rapid heat deposition at various target cross sections as well as in idealized axisymmetric geometries. These efforts have taken into account axially-and-radially varying transient heat deposition profiles in mercury and steel. A sample cross-section of the NSNS target where assessments are ongoing is shown in Fig. 12 along with indications of radial variations in transient energy deposition at this particular target cross section. Energy deposition occurs over 0.58 μs. Resulting transient pressures in the mercury and principal stresses in the target structure are shown in Fig. 13 for selected locations. It should be noted that the negative pressures in mercury shown in Fig. 13 for point 1 in Fig. 12 at a time of about 50 μs after the pulse imply that the mercury can support a rarefaction process. This result is an artifact of assuming a solid-like equation-of-state for mercury (Mie-Gruniesen form) and the presumption that liquid mercury will not cavitate. Onset of cavitation (either gaseous or vaporous) should produce significant reductions in system oscillations. However, it is recognized that related issues such as jetting and void generation-cum-collapse will need to be addressed. Developing a more realistic equation-of-state model for mercury in the regime expected in the SNS target is required to improve our understanding and predictive capability.

The minimum principle stress shown in Fig. 13 for the stainless steel container at the baffle (point 2 in Fig. 12) and external shell region (point 3 in Fig. 12) near the location with peak heating shows several characteristic time scales. For point 3, due to the significant impedane mismatches one notices short period (~ 1 μs) variations in stresses which are associated with the characteristic time scale for transfer of pressure waves through the thickness of the stainless steel structure and result in a "ringing" type effect. The longer time scale variations (tens of microseconds) for point 2 (superimposed with small oscillations) are due to the transport of pressure waves from the mercury to the baffle wall and transport through the steel. The resulting peak tensile stress in the stainless steel structure is found to be about -130 MPa. The (absolute) level of this stress is considerably below the yield stress of SS-316 steel. The acceptability of this stress level is not clear from a fatigue viewpoint, although existing data indicate that, with appropriate design modifications and optimization resulting loads should be manageable. It is recognized that, this stress must be examined in combination with other stresses and the dynamic (short duration) and cyclic (more than 10^8 cycles per month) nature of this stress must be appropriately considered along with the effects of irradiation.

4.4 Critical Issue and R&D Plans for the Mercury Target

Based mainly on the experience in operating mercury loops at the Institute of Physics in Riga, Latvia and the Center for MHD Studies at Ben-Gurion University in Beer-Shiva, Israel, it has been concluded that the technology for all mercury flow circuit components, excluding

1. the target itself,
2. spallation product related processing issues, and
3. specialized remote handling equipment,

already exists and is well understood and characterized. This means that the R&D program does not need to focus on liquid metal circuit components such as pumps, heat exchangers, valves, seals, and piping. R&D plans for the first item listed above, i.e., the target itself, have been formulated and are discussed below, whereas the design and analysis of the target are not mature enough to determine whether and what types of technology development are required for the other two items. Further design and analysis of the liquid metal target system is therefore needed to define flow circuit processing and remote handling equipment requirements and thereby identify any development needs.

The three main elements of the Mercury Target R&D program are:

1. Thermal shock tests and analyses

Fig. 12 CTH Model Schematic of NSNS Target Cross Section.

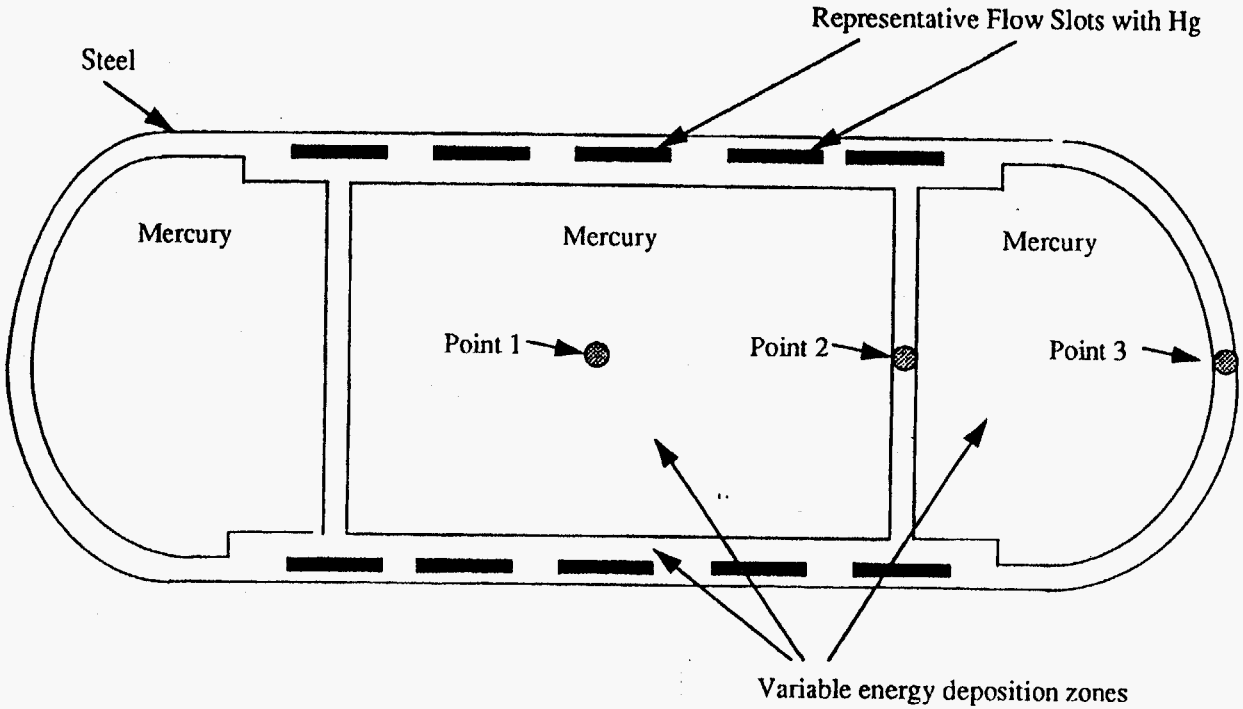

Notes (for 1-MW NSNS with 0.58 mic.sec. pulse):

1) Radial energy variation (= 0.83 MJ/g/s at center to 0.01 MJ/g/s at edges)
2) Mie-Gruniesen Equation-of-State (no cavitation)
3) Perfect contact of mercury with steel
4) Points 1, 2 and 3 are locations where pressure and stress variations are displayed in Figure 13.

Fig. 13 Variation of mercury pressure and stresses versus time at various locations (see Fig. 12) in NSNS target (1-MW case)

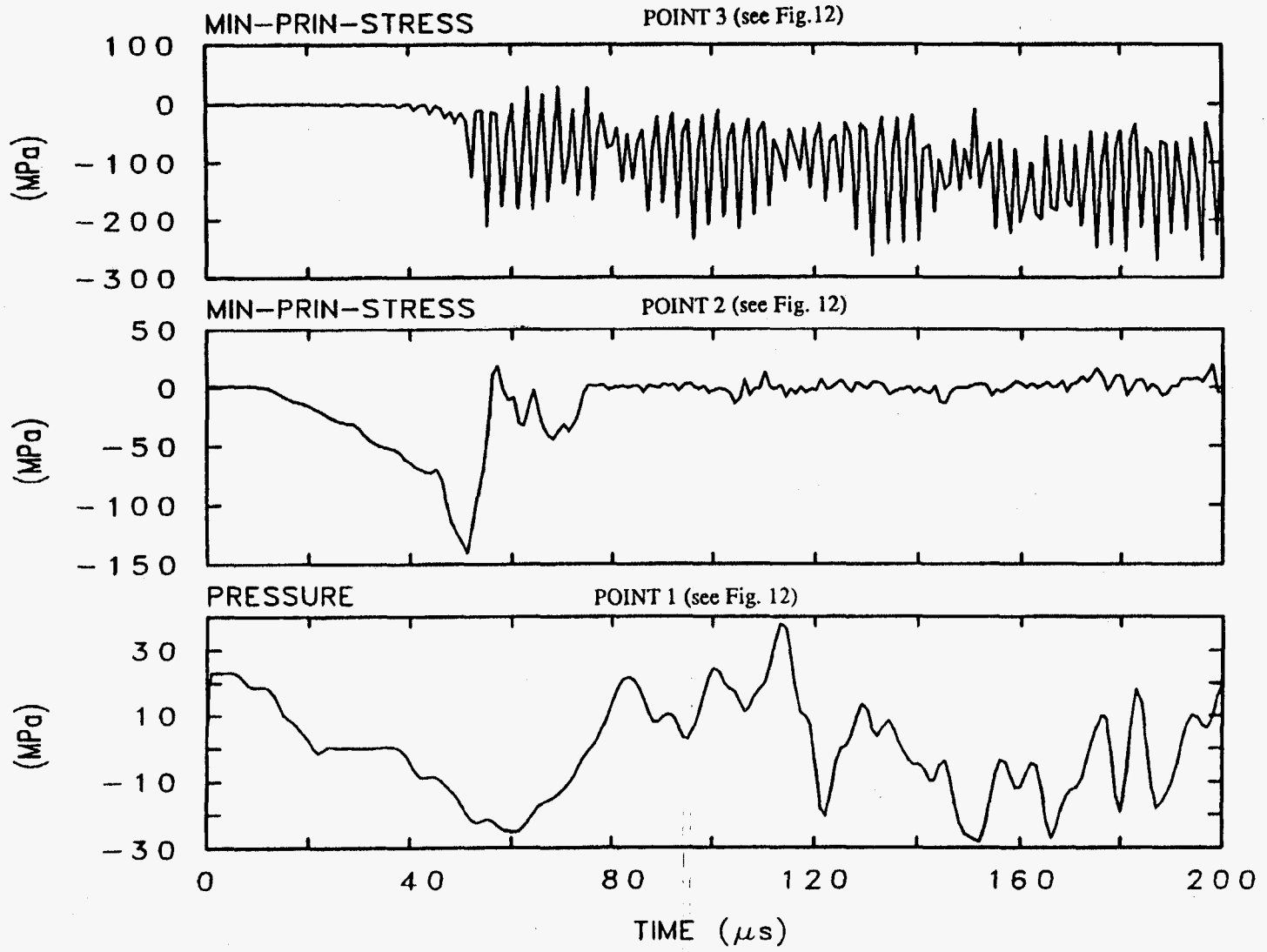

2. Thermal-hydraulic tests and analyses
3. Erosion/corrosion tests and analyses

Because of the challenges posed by the intense, pulsed thermal energy deposition (~10 kJ deposited during each ~1 μs pulse), the key feasibility issue that will be addressed in early R&D efforts is thermal shock. Simple pressure pulse tests and use of small-scale capsules of mercury in particle accelerator targets are planned for the near-term to improve our understanding of this phenomenon, and to benchmark and further develop our predictive models. Thereafter, effects on bulk fluid motion (e.g., surging), the impact and influence of engineered mitigative measures (e.g., possible use of helium bubble injection, etc.) and the effects of transient cavitation-cum-gas dissolution will need to be characterized for arriving at a qualified methodology for design applications.

Thermal-mechanical analysis and testing of the mercury target is also planned. The major issue associated with the thermal-mechanical performance of the mercury target is removal of the time-averaged power loading without excessive (1) temperatures in structural components or the mercury itself, (2) thermal stresses in the target structure, and (3) pressure drops in the flow circuit. The Thermal Hydraulic Tests and Analyses program is divided into six elements including: (1) computational fluid dynamics (CFD) simulation of the target, (2) creation of a central mercury handling system, (3) development of diagnostics and instrumentation for mercury, (4) flow distribution tests using water as a surrogate fluid, (5) mercury thermal hydraulic parameter tests, and (6) full-scale mercury tests with steady heat sources (no pulsed heating). All thermal-hydraulic testing is scheduled to be completed prior to the completion of the final design and fabrication of the target structure.

Testing is also required to establish that the mercury target system can operate with minimal corrosion of the target and its support equipment. Past experience with liquid metals, and in particular with mercury, has demonstrated that erosion of surfaces can be a problem for certain container materials. Furthermore, mercury corrosion has been shown to be greatly enhanced in flowing systems that have temperature differences in the flow loop. Corrosion is a concern for the mercury target system because it could potentially (1) lead to failure of the target vessel, (2) cause blockage of heat exchanger, valves, or other mercury coolant loop equipment due to transfer of corroded material from one region to another, or (3) lead to excessive contamination of mercury loop equipment due to transport of radioactively contaminated species from the target region to other regions in the mercury coolant loop. Following completion of materials compatibility tests, erosion/corrosion tests will be conducted on a full-scale thermal-hydraulic loop which will be assembled for the thermal-hydraulic tests discussed above.

5.0 MATERIALS TECHNOLOGY ISSUES FOR THE NATIONAL SPALLATION NEUTRON SOURCE TARGET STATION

High power spallation neutron sources like the NSNS will place significant demands on materials performance. The target system will be subjected to an aggressive environment that will degrade the properties of materials. Indeed, the satisfactory performance of materials for sufficiently long time periods will determine the viability of the target station for the facility. Components at the heart of the facility include the liquid target container and return hull, beam windows, support structures, moderator containers and beam tubes, for example. A recent workshop summarized the present state of knowledge of materials for spallation sources, and began implementing materials R&D programs for the NSNS and ESS facilities [Ref. 7]. The materials R&D program for the NSNS is oriented toward materials qualification. By this is meant informed selection of materials based on existing experimental data and analysis, testing in actual and partially simulated application environments, lifetime estimates for the NSNS environment, and iteration and optimization of properties to improve performance. The program is structured around technical areas expected to be key to the design, fabrication, and performance of the target station. The five overlapping areas can be termed radiation effects, compatibility, materials engineering, in-service surveillance and technical support.

Most of the present section will concentrate on radiation effects and compatibility. Materials engineering refers to the work necessary to translate knowledge gained in these areas into fabrication of components so that the necessary properties are achieved. Questions include, for

example, methods of welding and joining, assembly, heat treatments, and quality assurance. An in-service surveillance program is being developed to monitor and improve the performance of actual components. More importantly, standard specimens in a well-characterized environment that are more suitable than service components for testing and characterization will be irradiated. Parameters to be monitored include dose, dose rate, temperature, and target chemistry. The technical support function covers both the R&D phase of the project as well as the detailed design and construction phases. It gives a wide variety of support to the project that includes supplying materials properties data to target station engineers, and the solution of numerous applications-specific issues expected to arise.

5.1 Radiation Effects

Radiation effects issues are described from a somewhat general perspective here. A more complete background on this area is given in Reference 8, and a detailed description of areas of special relevance to spallation neutron sources is contained in References 7 and 9. The main problems in structural materials are expected to center around embrittlement, hardening and associated loss of ductility, and irradiation creep. Swelling at the modest temperatures currently under consideration for the NSNS, < 250 °C, is not likely to be a serious problem. Most experimental data on radiation effects in materials have been obtained in fission reactors. A limited amount of data from spallation neutron sources has also been accumulated. For example, some very low-dose information is available from neutron scattering targets removed from ISIS and LANSCE. Some higher dose data are available from the beam-stop experimental area of LANSCE. A new experiment is now under fabrication for irradiation in this facility to obtain moderate- and low-dose information on a number of materials intended for possible application in APT and NSNS. Supplementary information that is useful in technological investigations of radiation damage behavior is available from ion and electron irradiations in the few-MeV range.

By contrast to the few-MeV range of neutrons in fission reactors, materials in the NSNS will be exposed to protons in the GeV range and below, and to neutrons spanning from the proton energy down to thermal energies. The common unit of measure of displacement damage is the *displacement per atom, dpa.* One dpa is the dose at which, on average, each atom in the material has been displaced once. Required lifetimes of the most highly irradiated components such as the target nose, target container and beam windows are expected to be in the range of tens of dpa. Transmutation rates in the spallation environment will be orders of magnitude higher than in fission reactors. The species He and H, as well as heavier transmutation products will be of concern. H production is calculated to be in the range of 1000 appm/dpa. In particular, He production is calculated to be in the range of 100 to 200 appm/dpa as compared to 0.2 to 0.5 appm/dpa in fission reactors. Figure 14 shows graphically the He production rates in several neutron spectra. Helium is an insoluble rare gas that can increase the severity of radiation effects by triggering or increasing swelling, and by causing or exacerbating grain boundary embrittlement as well as hardening the material to promote overall ductility loss. The effects of the high He production will be determined in the present R&D program.

The NSNS is expected to operate in a pulsed mode. Most radiation effects data have been accumulated in steady conditions, albeit with interruptions for various reasons, but with no deliberate pulsing. During a pulse the instantaneous damage rate will be up to about 10^{-2} dpa/s. The highest available damage rate in fission reactors is approximately 10^{-6} dpa/s. In addition to the differences in microstructure caused by differences in instantaneous damage rates, the on-off cycle changes the kinetics of point defect buildup, which may result in changes in the accumulation of extended defects, such as dislocation loops. These changes in extended defect microstructure may therefore result in different mechanical properties than in steady irradiations. Some data is available from pulsed irradiations using ion accelerators [Ref. 10]. In that work it was found that pulsing at different pulse intervals caused changes in the sizes of dislocation loops, which would be expected to lead to changes in mechanical properties in a bulk specimen. These results were consistent with theoretical predictions for the effects of pulsing. More work may be required in this area to support the NSNS. However, in the long run an in-service surveillance facility will no doubt be the best source of information on the effects of pulsing.

Also shown in Fig. 14 is a special case encountered in mixed spectrum fission reactors. A few isotopes have high helium production cross-sections for thermal neutrons. For example, there is

the well known $^{10}B(n,\alpha)^{7}Li$ reaction, with the very high thermal reaction cross section of nearly 4,000 barns. This reaction has been used to study the effects of simultaneous He and damage production by adding boron to various materials. Of more interest for the stainless steels of intended application in the NSNS Hg container is the two step reaction $^{58}Ni(n,\gamma)^{59}Ni(n,\alpha)^{56}Fe$. In a stainless steel with nickel composition of about 15%, about 68% of which is ^{58}Ni in natural nickel, this reaction will produce the amount of helium as a function of dose shown by the dashed line in Fig. 14. This amount of He approaches half that expected in the spallation environment at high doses. Thus, mixed spectrum fission reactor irradiations can be utilized to provide relevant information on the effects of He on stainless steels irradiated in a spallation environment.

The planned experimental portion of the radiation effects R&D program for the NSNS consists of three parts. 1) Available spallation facilities at LANSCE and SINQ will be used for specimen irradiations. These will provide the most prototypic results, with the exception that pulsing will not be possible. In addition, the doses expected are only in the low to moderate range. 2) Special multiple beam irradiations will be carried out at the Triple Ion Facility at ORNL, Fig. 15. These will make possible the investigation of the effects of simultaneous damage and gas production, by bombarding with self-ions of the material such as Fe or Ni, and simultaneously injecting He and H at typical levels for a spallation environment. Results will reveal the effects on microstructures and give some applicable information on changes in mechanical properties by means of surface hardness tests. High doses will be achieved. Pulsing effects may also be investigated with these accelerators. 3) High dose neutron irradiations will be carried out in the HFIR reactor, making use of the helium production capability shown by the dashed line in Fig. 14. These reactor experiments will yield suitable specimens for true bulk mechanical testing, and give information on the effects of spallation-relevant simultaneous high dose and high helium accumulation. A combination of these three approaches will be required, since they give complementary information and none alone is adequate. The product of this work is the determination of acceptable parameter windows and estimated lifetimes for operation of the materials in the NSNS.

In parallel with the above experimental work, a program of modeling, analysis and computations is being carried out. This work is aimed at translating the calculated particle spectra into measures of the radiation damage to be experienced by materials and components. Important measures such as displacement damage, helium and hydrogen production rates, and transmutation rates of other species both in structural materials and in the Hg target are being calculated.

Fig. 14 Helium generation as a function of neutron fluence or displacement damage in several typical particle spectra in a stainless steel containing 15% nickel. The nickel two step reaction is responsible for the high helium production rate in a mixed neutron spectrum.

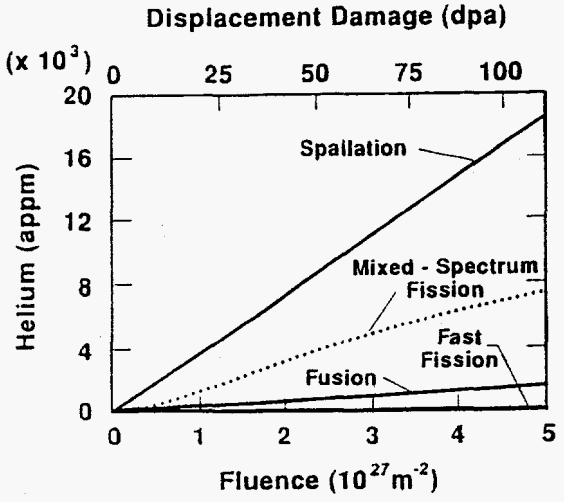

Fig. 15 The triple ion facility at Oak Ridge National Laboratory, where specimens can be exposed simultaneously to beams of Fe, He, and H, for example.

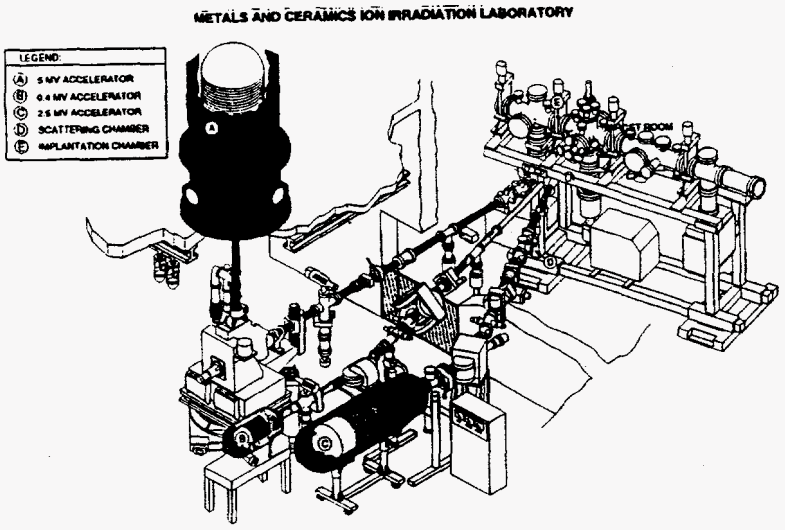

Wherever possible, calculations will be compared with experiments. For example, helium contents of materials irradiated in LANSCE or SINQ will be measured and compared with predictions.

5.2 Compatibility

This effort addresses the compatibility and corrosion behavior of materials in contact with liquid Hg, such as the container and flow baffles. The work also covers issues in associated water cooled systems. Previous experience in liquid metal systems has been evaluated for its applicability to the present system. An R&D program for mercury compatibility with containment materials is presently in progress. An up-to-date background on this area is contained in the proceedings of a recent workshop (Ref. 11). In water systems there is already a large amount of experience. Considering this and the fact that water systems will be auxiliary systems rather than the heart of the target itself, it is considered that only a minimal level of R&D is required for water compatibility issues. The main issues in the Hg systems are considered to be temperature gradient mass transfer, liquid metal embrittlement, and wettability of materials by Hg (Ref. 12). Experimental evaluation now underway includes constant extension rate tensile tests for liquid metal embrittlement (LME) and rocker tests for temperature gradient mass transfer. Further testing is planned to include notched tensile and fatigue tests in mercury as well as small scale recirculating loop tests. This work interfaces closely with related engineering R&D on thermal hydraulics and mechanical design. In particular, it supports planned work on more prototypic large scale and high flow rate engineering test loops.

In temperature gradient mass transfer, material in higher temperature portions of a circulating system is removed and deposits in lower temperature regions. This effect can be large and may lead to narrowing and even blockage of flow paths. Important parameters include operating temperature T, the ΔT between various parts of the system, solubility of alloy components in the liquid Hg as a function of temperature, solution and deposition rate constants, and flow rate. In austenitic stainless steels, the primary candidate material for the mercury container, Ni may dissolve preferentially from the alloy and thus be of concern for temperature gradient mass transfer. Keeping the operating temperature of the system below about 250°C, however, is expected to reduce this effect to an acceptable level. Part of the R&D effort is to determine quantitatively the $T/\Delta T$ windows that are acceptable for this application.

The "rocker" test was devised for screening materials and $T/\Delta T$ combinations for temperature gradient mass transfer. Figure 16 is a schematic of this apparatus. One end of a dog-

bone shaped mercury-containing chamber is surrounded by a furnace. The other end is surrounded by room temperature air. Specimens of the material of interest are contained in each chamber. The configuration is rocked from end to end at intervals of minutes, alternately exposing one specimen to hot mercury and the other to cooler mercury. After testing, specimens are examined and weighed to determine mass transfer. Results of the first rocker tests are summarized in Table 5. In general, weight changes were very slight, and the addition of magnesium to the mercury did appear to promote wetting of the steel.

Fig. 16 Rocker test configuration for screening materials with respect to temperature gradient mass transfer.

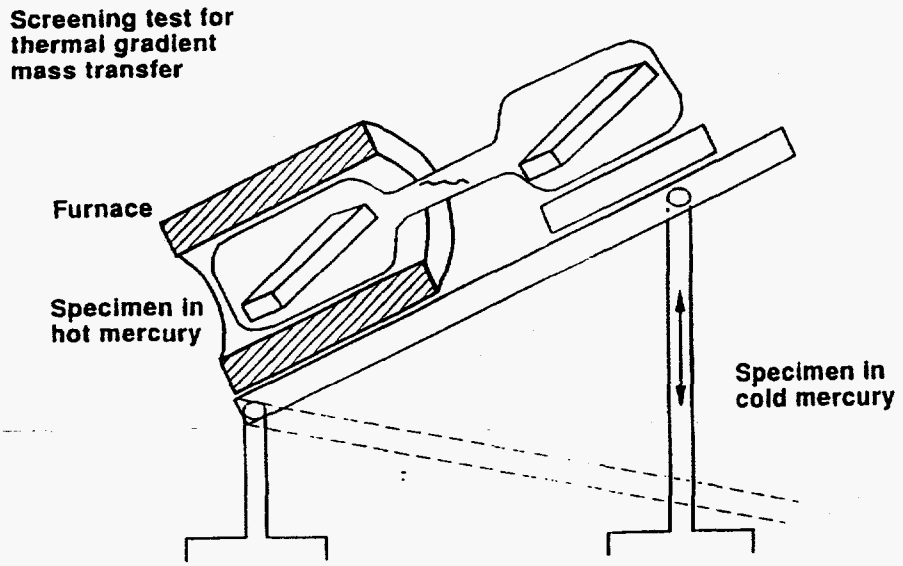

Liquid metal embrittlement (LME) is being investigated using constant extension rate tensile tests. Wettability can be examined as well by varying the Hg chemistry. Generally, it is expected that when Hg wets the material, liquid metal embrittlement is possible, although not inevitable. When there is no wetting it is thought that LME is not possible, although efficient heat transfer may then become a problem. Both embrittlement and wetting are being examined as a function of temperature and of chemistry by adding solutes to the mercury. Results of tests completed thus far are summarized in Table 6. No liquid metal embrittlement effects were noted, primarily measured by total elongation and reduction of area, and the addition of small amounts of gallium to mercury increased wetting of the type 316 stainless steel.

6.0 CONCLUSIONS

Preliminary design and analysis indicate that a very attractive short-pulse neutron source operating at 1 MW of proton beam power can be constructed for the NSNS using liquid mercury as the target material. Research and development activities have been identified to validate design concepts and to allow future upgrades to higher power levels. Reasonable design configurations have been proposed for major component assemblies and remote handling concepts have been

developed. A complete description of the NSNS project can be found in the Conceptual Design Report. [13]

Table 5 Results of initial rocker screening tests of type 304SS in mercury

Average maximum temperature: 300 °C Average DT: 78°C Time: 2,000 h Cycles (60s/18s): 92,000						
Capsule environment	Mg in Hg	Visual wetting Hot	Visual wetting Cold	Weight change, mg/cm^2 Hot	Weight change, mg/cm^2 Cold	Comments
Air	None	No	Yes	-.14-	.12	Hg fairly bright and shiny
He	None	No	No	-.14	-.02	Hg very bright and shiny
Vac	None	Yes	Yes	-1.53	+.004	Deposit on cold leg surface
Air	100 ppm	No	Yes	-.04	-.02	Dark residue in Hg
He	100 ppm	Yes	Yes	-.92	-.03	Dark residue in Hg

Table 6 Results of LME constant extension rate tensile tests on 316SS

Environment	Strain rate (cm./cm.s)	Strength Yield (Mpa)	Strength Ultimate (Mpa)	Reduction in area (%)	Total elongation (%)	Comments
Air	9.5×10^{-6}	376	664	78	32	
Hg[a]	9.6×10^{-6}	364	673	72	30	Little or no wetting
Hg + 1% Ga[a]	9.4×10^{-6}	393	673	80	33	Sample wet
Air	4×10^{-3}	4.35	659	75	24	
Hg + 1% Ga[a]	7×10^{-3}	4.35	687	77	30	Sample wet
[a]Ultrasonically agitated prior to test (to promote wetting).						
Future LME tests include: • Sensitized 316SS • Welded 316SS • Fatigue						

REFERENCES

1. T. A. Gabriel et al., "CALOR87: HETC87, MICAP, EGS4, and SPECT, A Code System for Analyzing Detectors for Use in High Energy Physics Experiments," Proceedings of the Workshop on Detector Simulation for the SSC, Argonne National Laboratory, August 24-28, 1987.

2. J. F. Briesmeister, Ed. "MCNP - A General Monte Carlo Code for Neutron and Photon Transport," Los Alamos Scientific Laboratory Report LA-7396-M, Rev. 2 (September 1986).

3. J. M. Carpenter and W. B. Yelon, "Neutron Sources," Methods of Experimental Physics, Vol. 23A, (1986) 99.

4. C. J. Westcott, Chalk River Report CRRP 960 (Revised 3rd addition) (1970)

5. "CFX 4.1 Flow Solver User Guide," Computational Fluid Dynamics Services, AEA Technology, Harwell Laboratory, Oxfordshire, United Kingdom, October 1995.

6. J. M. McGlaun and S. L. Thompson, "CTH-A Three Dimensional Shock-Wave Physics Code, "Intl. Journal of Impact Engineering," Vol. 10, 251-360,1990.

7. L. K. Mansur and H. Ullmaier, Proceedings of the International Workshop on Spallation Materials Technology, April 23-25, 1996, Oak Ridge, Tennessee, CONF-9604151.

8. L. K. Mansur, "Theory and Experimental Background on Dimensional Changes in Irradiated Alloys," J. Nucl. Mater. 216 (1994) 97-123.

9. L. K. Mansur, "Radiation Materials Science and Technology for Spallation Neutron Sources," presented at the Symposium on the Savannah River Accelerator Project and Complementary Spallation Neutron Sources, Columbia, SC, May 14-15, 1996.

10. E. H. Lee, N. H. Packan, M. B. Lewis, and L. K. Mansur, "Effects of Rapidly Pulsed Ion Bombardment on Microstructure and Phase Stability in a Ti-modified Stainless Steel," *Nucl. Inst. and Meth.* **B16** (1986) 251-259.

11. B. R. Appleton and G. S. Bauer, Proceedings of the International Workshop on the Technology and Thermal Hydraulics of Heavy Liquid Metals (Hg, Pb, Bi, and their Eutectics), March 24-29, 1996, Schruns, Austria, CONF-9603171.

12. a) J. R. DiStefano and S. J. Pawel, "Compatibility of Materials with Liquid Metal Targets for SNS Applications," in Ref. 11.

    b) J. R. DiStefano, S. J. Pawel, and J. H. DeVan, "Mercury Compatibility Issues for ORSNS," in Ref. 7.

13. NSNS Conceptual Design Report, in press, Oak Ridge National Laboratory, June, 1997.